STScI | SPACE TELESCOPE SCIENCE INSTITUTE

Instrument Science Report COS 2018-24(v1)

Improvements to the COS FUV G130M and G160M Wavelength Solutions at Lifetime Position 3

Rachel Plesha[1], Thomas Ake[1,2], Gisella De Rosa[1], Cristina Oliveira[1], Steven Penton[1,3]

[1] Space Telescope Science Institute, Baltimore, MD
[2] Latitude, Inc.
[3] Laboratory for Atmospheric and Space Physics, University of Colorado Boulder

18 March 2019

ABSTRACT

The wavelength dispersion coefficients and zero points of the COS FUV G130M and G160M gratings at each lifetime position (LP1, LP2, LP3, LP4) have been re-derived. Unlike the previous derivations for LP1 and LP2, which used archival data only, special calibration programs were executed at LP3 to obtain wavelength calibration data as well as new lamp spectra to create a lamp template specific to LP3. The wavelength solution accuracy has been improved from $\sim$ 15 km s^{-1} (6 pixels) to $\sim$ 7.5 km s^{-1} (3 pixels). Here we present the results and methodology behind deriving the wavelength calibration solutions specific to LP3. Discussions of the methodology used to derive updated wavelength solutions at lifetime positions 1, 2, and 4 are presented in separate documents.

Contents

1. Introduction

On February 9, 2015, the nominal FUV spectrum location was changed from Lifetime Position 2 (LP2) to Lifetime Position 3 (LP3) (Roman-Duval et al. 2016) to mitigate gain-sag effects from cumulative exposure usage (Sahnow et al. 2011). Monitoring at LP3 for the G130M and G160M gratings showed that the wavelength accuracy requirement of $\pm$ 15 km s^{-1}, or about one resolution element, was still being met (Sonnentrucker 2017). Since then, calibration efforts have been made to improve the wavelength accuracy at the first Lifetime Position (LP1) and at LP2 to half a resolution element, or $\sim$ 7.5 km s^{-1}, as discussed in Plesha et al. (2018) and Ake et al. (2019) respectively. We present here a similar study to achieve this accuracy at LP3.

The wavelength solutions for COS can be found in the dispersion relation reference file (DISPTAB) and are defined using the equation:

$$\lambda = a_0 + a_1 \times x_{prime} + a_2 \times x_{prime}^2, \tag{1}$$

where x_{prime} is calculated from XFULL pixel coordinates (thermally, geometrically, drift, and FP-POS corrected) and zero-point offsets between those derived on orbit (d) and PSA-to-WCA offsets derived in thermal vacuum (TV) testing (d_{TV03}):

$$x_{prime} = XFULL + d_{TV03} - d \tag{2}$$

(Oliveira et al. 2010). In the FUV channel, the medium-resolution grating wavelength solutions are linear (a_2 = 0). Additionally, since the new calibrations presented here are based solely on PSA data obtained on orbit, the zero-point offsets between the PSA and WCA are not needed and $d = d_{TV03} = 0$, so x_{prime} = XFULL. In this study, we have derived both a_0 and a_1 for the G130M and G160M standard cenwaves at LP3. We used a cross-correlation technique, as performed for LP1 and LP2, that aligns COS spectra to STIS echelle spectra of the same target to derive zero points and dispersion coefficients. We use STIS observations as a reference spectrum because of their higher wavelength accuracy. The absolute wavelength accuracy of the STIS echelles is $\sim$ 2 km s^{-1}, compared to the current COS wavelength accuracy of $\sim$ 15 km s^{-1}. The goal was to

increase the FUV wavelength accuracy to $\sim$ 7.5 km s^{-1}, i.e., from one COS resolution element (6 pixels) to half a resolution element (3 pixels). More details can be found in the LP1 FUV wavelength calibration ISR (Plesha et al. 2018).

On April 9, 2018, the DISPTAB 24914346l_disp.fits and lamp template reference file (LAMPTAB) 24914347l_lamp.fits were released for use jointly at LP3. The new lifetime-dependent LAMPTAB was created to further improve the wavelength solution accuracy through more accurate comparisons between the templates and TAGFLASH exposures in the wavelength correction step of the COS calibration pipeline, CalCOS. The LP3 LAMPTAB was created using data from PID 14856. Since the lamp templates define the reference frame for the wavelength solutions, the new DISPTAB and LAMPTAB must be used together. For more details about how the lifetime-dependent LAMPTAB reference files were created, see E. Frazer et al. (2019, in prep.).

As with LP2 (Ake et al. 2019), data available in the archives for LP3 were inadequate to employ all of the same analyses as had been performed at LP1. Few targets had been observed with both COS and STIS, and several cenwaves had not been used at all. Because of this, a calibration program (PID 14909) using the targets ϵ Eri and AV 75 was created to derive the wavelength solutions. The details of the program are discussed in Section 2. Section 3 describes the methodology used to derive the wavelength solutions for the G130M (1291, 1300, 1309, 1318, 1327) and G160M (1577, 1589, 1600, 1611, 1623) cenwaves. The final results for all LP3 modes are shown in Section 4. In late 2018, after all of the analyses were completed, it was decided that the G130M/1222 setting at LP3 should be updated with the solutions derived at LP4 to improve their wavelength accuracy as well. The results of this separate analysis are discussed in Section 5. Finally, the details specific to the reference files are outlined in Section 6.

2. Program Details

Unlike for LP1 and LP2, there was a shortage of COS and STIS data of the same target to derive wavelength solutions for the COS FUV cenwaves at LP3. Because of this, a calibration program designed specifically to derive wavelength solutions for the G130M and G160M standard cenwaves at LP3 was created (PID 14909). Since the program was designed specifically to derive wavelength solutions, the observed target or targets needed to have a plethora of bright features that sufficiently covered both FUVA and FUVB detector segments. Additionally, to reduce any centering errors introduced into the wavelength solutions by using only one target, a precise target acquisition needed to be a part of the program. In the LP1 and LP2 solutions, any centering error due to the target acquisition was minimized by using multiple targets, each with their own target acquisition, for each cenwave (Plesha et al. 2018). Finally, in order to tie the COS wavelength scale to that of STIS, the object would also need to be bright enough to observe with STIS echelle modes in a reasonable length of time, yet be faint enough to observe with COS.

After a review of targets used at LP1 and LP2 as well as other potential candidates, the bright K2Vk star ϵ Eri was selected as the primary target. As a chromospherically active star, it has a myriad of emission lines that have been well studied in the FUV (e.g., Sim & Jordan 2003 for STIS, France et al. 2016 for COS). Its radial velocity has been extensively monitored (e.g., Giguere et al. 2016), indicating variability < 20 m s^{-1} and a small rotation rate ($v \sin i < 3$ km s^{-1}). For the LP2 wavelength solution, ϵ Eri provided $20-40$ measurable features per segment for each grating (although not observed with G130M/FUVB) and had sufficient segment coverage to reveal an unrecognized bump in wavelength residuals at the short wavelength end of FUVA, due presumably to walk effects and/or geometric correction error (Ake et al. 2019). Some late-type dwarfs show small emission-line velocity shifts related to the formation temperature of the species (e.g., Redfield et al. 2002), but this is of little concern to the COS wavelength calibration since any shifts appear in the STIS spectra as well. The main disadvantage for this object, as well as other emission-line candidates, is that the Ly α count rate is too high for the COS FUV detectors. Therefore, another target had to be used to cover G130M/FUVB. The O5.5I(f) star AV 75 was selected because it has sufficient ISM lines for the segment and has been used in the yearly wavelength calibration monitoring program. Additionally, to check that there were enough features to cover the FUVB detector with AV 75, we re-derived the LP2 G130M wavelength solutions using only the AV 75 data available at that lifetime position, which consisted of cenwaves 1291, 1309, 1327. Even missing two cenwaves, we were able to accurately re-derive the delivered wavelength solution that we obtained from multiple targets for LP2 (Ake et al. 2019).

Program 14909 consisted of three visits. Visits 01 and 02 observed ϵ Eri, and Visit 03 observed AV 75. Table 1 lists the COS exposures. The first two visits used the most accurate target acquisition pattern available, which is two consecutive NUV imaging acquisitions. Long exposures (2722 s) were obtained for the extreme and middle cenwaves (1291, 1309, 1327, and 1577, 1600, 1623) to accurately fit the dispersions to the ray-trace models, and the remainder of each visit was filled with shorter exposures ($\sim$ 900 s) for the other two standard cenwaves per grating, i.e., 1300, 1318, 1589, and 1611, to obtain the correct zero points. All data were taken at FP-POS = 3.

Visit 03 obtained data of the target AV 75 for the G130M cenwaves 1300, 1309, 1318, and 1327 of equal exposure time (320 s). Data from previous LP3 wavelength calibration monitoring programs (13931 [v51], 14437 [v51], 14855 [v01]) were deemed to be adequate to derive the 1291 solution. Visit 03 was rescheduled as visit 3A due to an unrelated SIC&DH lockup of HST that occurred shortly before the visit was scheduled to execute and therefore prevented the visit from executing. This changed the target acquisition that was to be used but otherwise did not change the visit structure. The original BOA ACQ/SEARCH + ACQ/IMAGE contained orientation constraints that excluded several bright stars in the field. The updated target ACQ/SEARCH + ACQ/PEAKXD + ACQ/PEAKD used G130M/1300 with the PSA instead.

Table 1. List of Exposures for Program 14909

Target	Grating	Cenwave	ObsID	Start Time (UT)	Exposure Time (s)
ϵ Eri	G130M[1]	1300	ldej01hmq	2017-03-07 06:33:08	928
		1318	ldej01hrq	2017-03-07 06:51:47	929
		1291	ldej01ifq	2017-03-07 07:57:19	2722
		1309	ldej01iiq	2017-03-07 09:33:10	2722
		1327	ldej01ikq	2017-03-07 11:12:00	2722
	G160M	1589	ldej02g0q	2017-03-12 04:13:19	908
		1611	ldej02g3q	2017-03-12 04:31:38	909
		1577	ldej02g8q	2017-03-12 05:36:49	2722
		1600	ldej02ggq	2017-03-12 07:12:12	2722
		1623	ldej02goq	2017-03-12 08:47:36	2722
AV 75	G130M	1300	ldej3aktq	2017-04-04 13:43:59	320
		1309	ldej3akvq	2017-04-04 14:35:01	320
		1318	ldej3akxq	2017-04-04 15:14:56	320
		1327	ldej3akzq	2017-04-04 16:10:20	320

[1]Segment FUVA only.

3. Methodology

To derive the LP3 wavelength solutions, the techniques outlined in Plesha et al. (2018) and Ake et al. (2019) were used. A cross-correlation was performed between COS data and STIS echelle spectra resampled and convolved with the appropriate LP3 COS LSFs. As with LP1 and LP2, the flux-weighted centroid of each of the defined spectral features in COS pixel (XFULL) space was measured, and, by comparing to the known wavelength scale of STIS, new linear dispersion and zero-point coefficients were computed by performing a least-squares fit of XFULL values to geocentric wavelengths. The resulting dispersion coefficients were then fit to ray-trace models by performing a χ^2 fit of the dispersion versus Optics Select Mechanism 1 (OSM1) focus position. Despite limited archival data, we were able to test the co-alignment of the cenwaves using data from other targets. However, we decided not to apply the minor zero-point offsets for reasons discussed in more detail in Section 4.2. In section 3.1 we briefly discuss the creation of a new lifetime-dependent LAMPTAB. The investigation into the variability of ϵ Eri is discussed in Section 3.2.

3.1 New LAMPTAB

Starting with LP3, a lifetime-specific LAMPTAB was created along with the new DISPTAB to improve the resulting shifts found in the wavelength correction step of the COS calibration pipeline, CalCOS. Previously, the lamp templates used were derived

from observations at LP1, obtained during SMOV. Although similar, the lamp spectrum changes with lifetime position, so by using a template from LP1 at LP3, errors were introduced into the wavelength accuracy error budget. Furthermore, the LP1 lamp templates do not account for any new localized detector features, changes in lamp intensity, or gain-sagged regions that can occur when observations are moved to a new lifetime position. The LP3 LAMPTAB, 24914347l_lamp.fits, should be used exclusively with the LP3 DISPTAB, 24914346l_disp.fits because the zero points are anchored to the specific OSM1 position of the new LAMPTAB. Details of how this LAMPTAB was created can be found in E. Frazer et al. (2019, in prep.).

3.2 Variability of ϵ Eri

As a chromospherically active star, ϵ Eri is well known to show short- and long-term cyclical variability both photometrically and in Ca II H & K emission line strengths. Star spot measurements show an 11 d rotation period and long-term solar-cycle-like behavior with periods on a 3–13 yr timescale that is related to dynamo activity. However, H & K emission does not correlate with radial velocity changes (Howard & Fulton 2016), which nonetheless are much smaller than what COS can detect. On shorter timescales, Audard et al. (2000) have characterized coronal flare activity in the EUV region.

Figure 1 shows a timeline of the count rates of Si IV 1393 Å (G130M) and C IV 1548 Å (G160M) to check for short-term activity during the exposures. Two prominent flares, $\sim$ 2–3 times quiescence, are visible along with less prominent ones. To look into the impact of the variability on the wavelength calibration, the count rates of lines located in all windows used for the cross-correlations with STIS data were examined. Figures 2 and 3 show a light curve for each window defined for the calibration, for G130M and G160M respectively. It is clear that only some of the spectral lines are varying within an exposure, some with obvious flare signatures, a few with more subtle variations. Out of 107 total defined features across the entire G130M and G160M wavelength range for ϵ Eri, only 12 were found to be variable and are listed in Table 2.

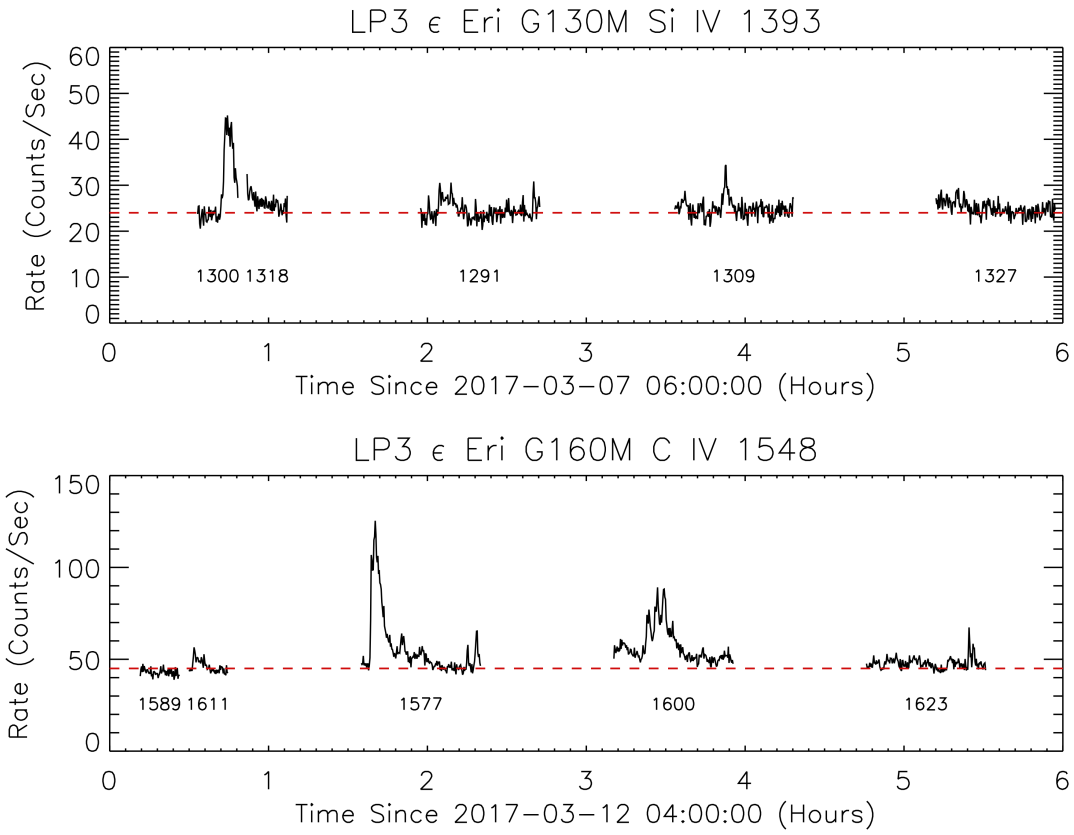

Figure 1. Count rate variability during the two ϵ Eri visits. Cenwaves are noted below the data for each exposure. Net count rates for the G130M grating are for Si IV 1393 Å and for the G160M grating are for C IV 1548 Å. The red dashed lines are the average quiescent levels.

The Si IV and C IV line profiles during the largest flares were investigated next. These had sufficient counts to separate the flare and quiescent line shapes and provide data to determine the overall effect of variability on wavelength measurements. Figure 4 shows the light curves and time-resolved profiles, where we have isolated the flare between the rise and decay half-power points (where the variability should have most of the effect) and the quiescent state (times completely outside the flaring period). For the Si IV flare, the rise time is more gradual than for the C IV one and the flare spectrum affected only the base of the quiescent profile. For the C IV flare, which had two peaks, there is a line shift and redward extension to the flares. Even though the flare peak was brighter than the quiescent state, the profile integrated over the whole exposure still had only a small wavelength shift since the basal flux level at quiescence is preponderant. At the COS resolution, we expect other lines are affected even less. Table 2 shows the measured spectrum shifts due to flaring for the variable features. Although the shifts are all smaller than a pixel, these windows were excluded from the wavelength solution.

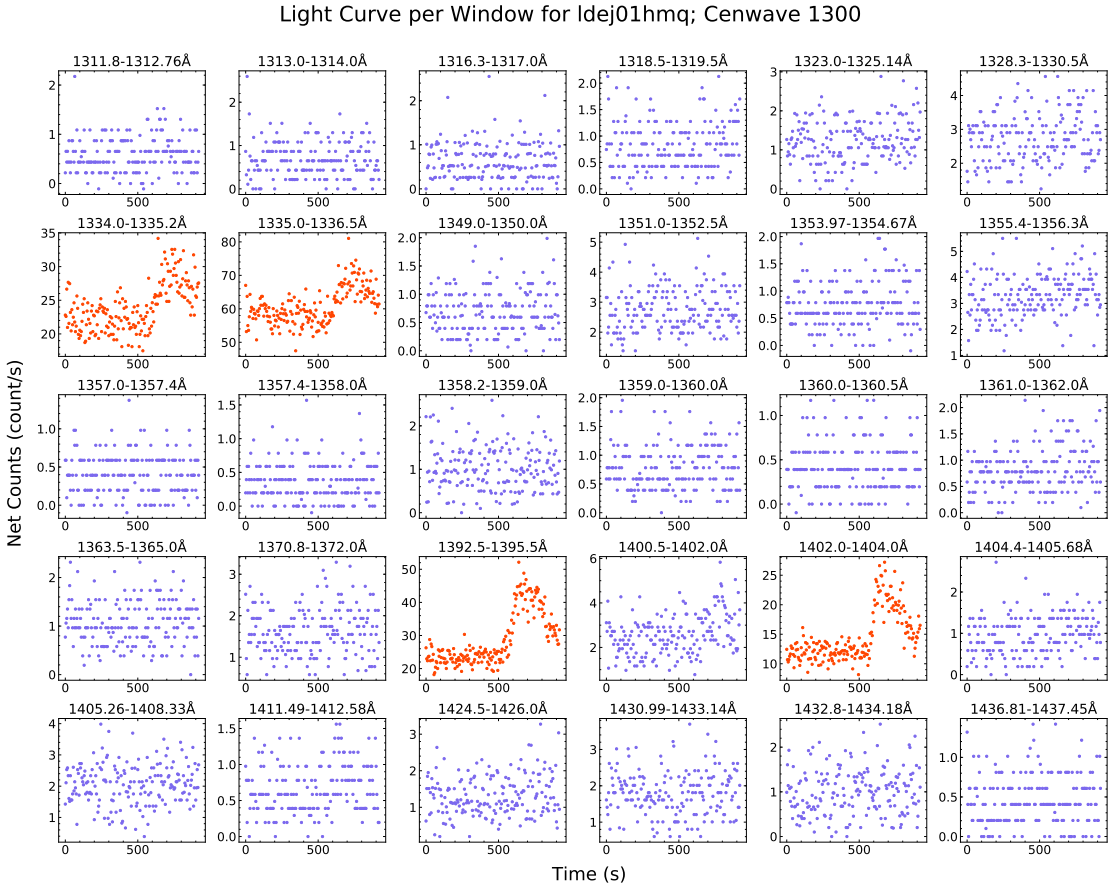

Figure 2. Light curves for each defined window that falls within the G130M/1300 wavelength range for FUVA that was not excluded from the analysis due to an SDQ flag. Most windows do not show any variability (purple), but there are a few that have peaks indicative of flare activity (red) in ϵ Eri, such as Si IV in the 1402−1404 Å window.

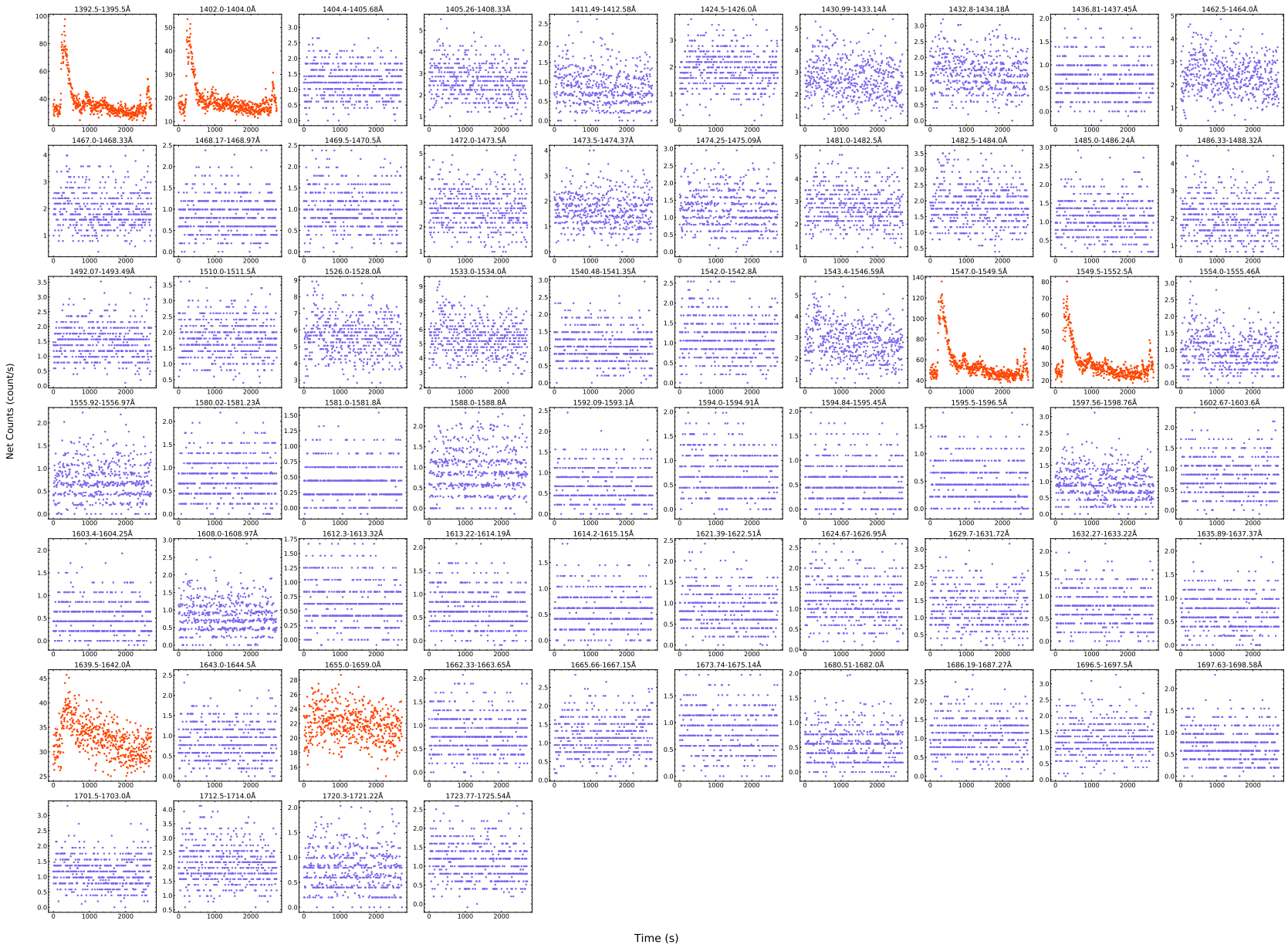

Figure 3. Same as Figure 2, but showing the windows covered by G160M/1577. Both segments are covered by G160M unlike G130M, for which only FUVA data of ϵ Eri is available. Windows in red indicate a variable feature. In this exposure, the 1655−1659 Å window is not showing variability but was still excluded from the analysis because it showed variability in a different exposure. The majority of the defined windows do not contain variable features.

Table 2. Variable Spectral Windows in ϵ Eri and Shifts between Quiescent and Total Profiles for the Two Largest Flares

Wavelength Minimum (Å)	Wavelength Maximum (Å)	Ion	Shift 1300 (pixels)	Shift 1577 (pixels)
1293.16	1295.51	Si III		
1296.31	1298.06	Si III		
1298.00	1300.00	Si III		
1334.00	1335.20	C II	0.05	
1335.00	1336.50	C II	0.01	
1392.50	1395.50	Si IV	−0.29	0.48
1402.00	1404.00	Si IV	−0.46	0.63
1547.00	1549.50	C IV		0.78
1549.50	1552.50	C IV		0.77
1639.50	1642.00	He II		0.29
1655.00	1659.00	C I		
1772.00	1773.30	Fe II		

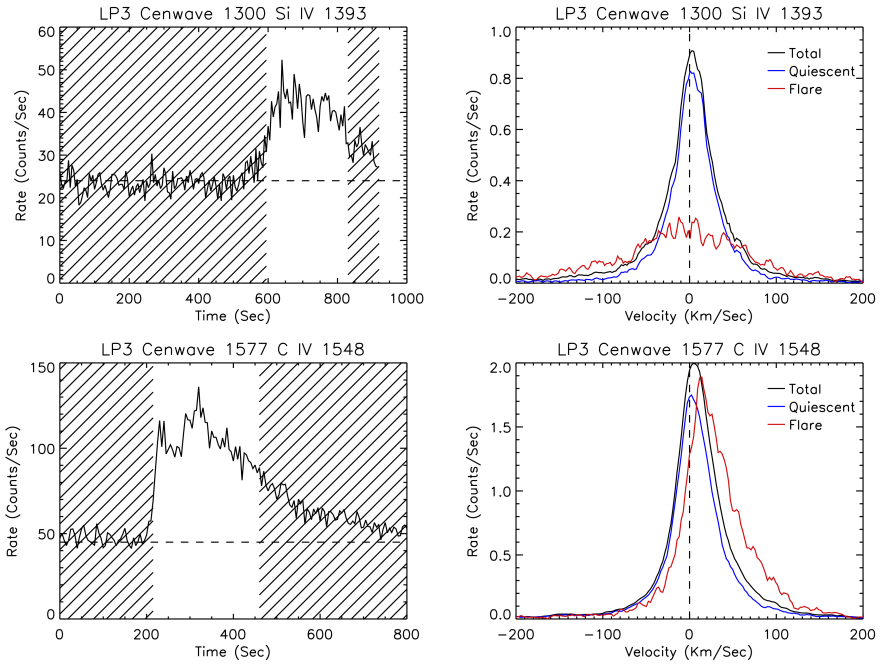

Figure 4. Light curves and spectra for the two largest ϵ Eri flares. Upper panels are Si IV 1393 Å during the G130M/1300 exposure; the lower are C IV 1548 Å from G160M/1577. Hatched areas are data excluded from the flare spectra, which were integrated between the half-power rise and decay levels. In each case the count rate in quiescence has been subtracted from that during the flare period. The total profile includes all data taken during the exposure.

4. Results

A new DISPTAB, 24914346l_disp.fits, was released on April 9, 2018 for use with data at LP3. Table 3 lists the updated, rounded dispersion zero points (a_0) and coefficients (a_1). The full values can be found in the DISPTAB reference file. The COS-to-STIS data were tested in the same manner as for LP1 and LP2 (Plesha et al. 2018, Ake et al. 2019). The results are shown in Section 4.1. However, the COS-to-COS cross-correlation analysis discussed in Section 4.2 differed from LP1 and LP2 due to the lack of COS data with overlapping cenwaves within the same visit.

Like for LP2 (Ake et al. 2019), the dispersion coefficients were compared to OSM1 focus position. The derived LP3 dispersion coefficients are shown versus OSM1 focus position in Figure 5 with LP1 and LP2 overlaid for comparison. When the focus mechanism is repositioned, as is done for every lifetime position move, the dispersion changes. For FUVB, all three lifetime positions seem to follow nearly the same dispersion relation. For FUVA, however, we find that LP3 is offset from LP1 and LP2.

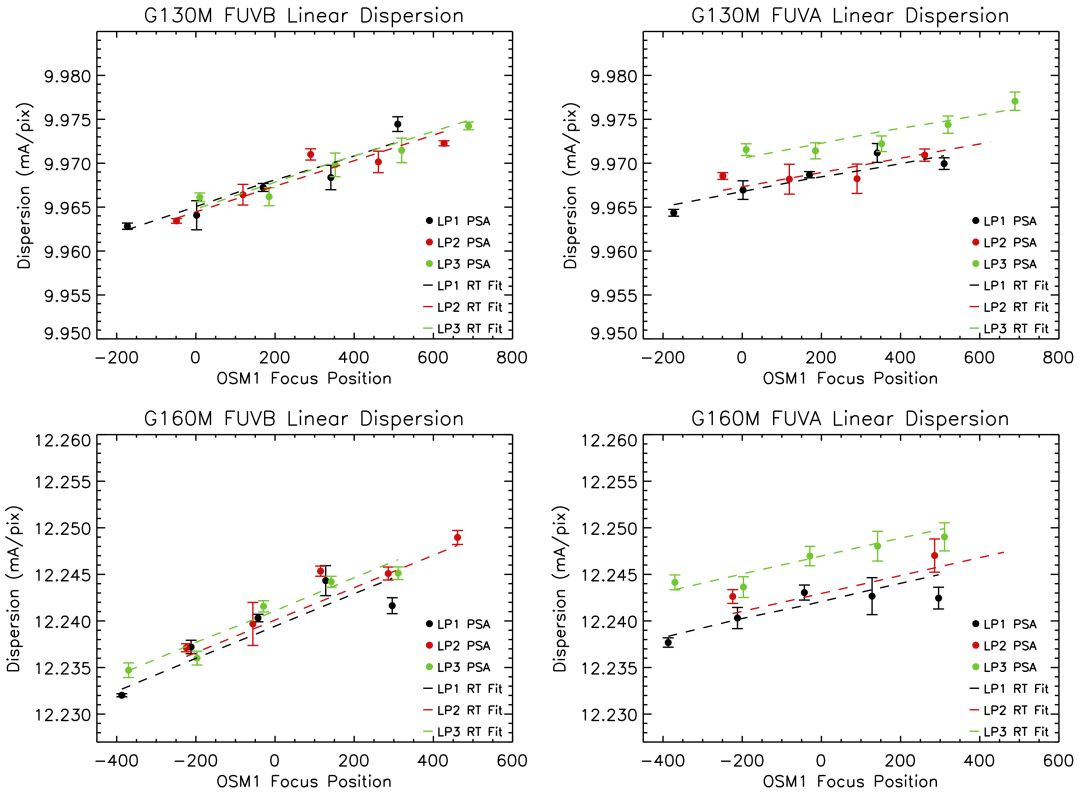

Figure 5. Dispersion coefficients versus OSM1 focus position for LP1 (black), LP2 (red), and LP3 (green). Each solid circle represents a cenwave, increasing from left to right starting with 1291 or 1577, for a given lifetime position. Dashed lines are the corresponding values from the ray-trace models that were adopted for each cenwave.

Table 3. Rounded, Updated Zero Points (a_0) and Dispersion Coefficients (a_1) for LP3 Modes[1]

Grating	Cenwave	Segment	a_0 (Å)	a_1 (10^{-3} Å pix^{-1})	Segment	a_0 (Å)	a_1 (10^{-3} Å pix^{-1})
G130M	1291	FUVA	1278.220	9.9706	FUVB	1125.015	9.9649
	1300	FUVA	1287.846	9.9721	FUVB	1134.619	9.9676
	1309	FUVA	1297.534	9.9736	FUVB	1144.260	9.9702
	1318	FUVA	1307.049	9.9748	FUVB	1153.736	9.9725
	1327	FUVA	1316.642	9.9762	FUVB	1163.288	9.9749
G160M	1577	FUVA	1562.953	12.2434	FUVB	1374.868	12.2347
	1589	FUVA	1574.732	12.2451	FUVB	1386.591	12.2378
	1600	FUVA	1586.176	12.2467	FUVB	1397.988	12.2406
	1611	FUVA	1598.046	12.2484	FUVB	1409.809	12.2436
	1623	FUVA	1610.132	12.2499	FUVB	1421.850	12.2466

[1]The DISPTAB should be consulted for the exact values.

4.1 COS-to-STIS Comparison

As with the other lifetime positions, we reprocessed the COS data used to derive the wavelength solutions with the newly derived DISPTAB, along with the new LAMPTAB, for LP3. A cross-correlation between the resultant spectra and the LSF-convolved STIS data was performed again. This allowed us to check whether the ray-trace solutions yielded any residual zero-point shifts or other anomalous behavior compared to the individual solutions for each cenwave. As shown by the black stars in Figures 6 and 7, the LP3 solutions now meet the improved wavelength accuracy goal of ± 3 pixels ($\sim$ 7.5 km s^{-1}).

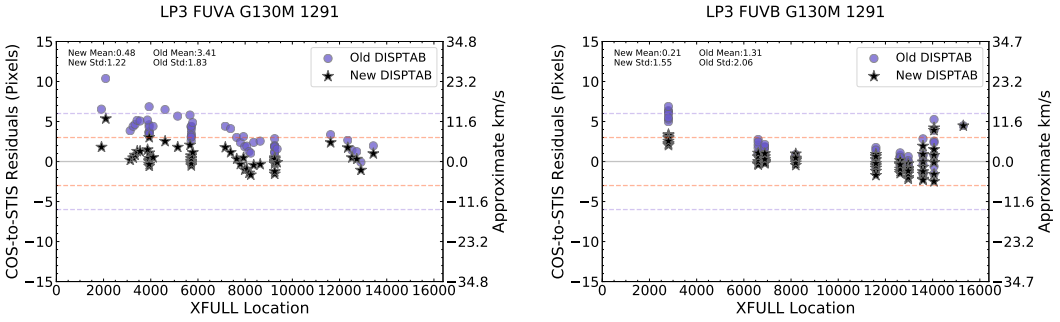

Figure 6. COS-to-STIS cross-correlation residuals for G130M, all updated cenwaves and segments. The residuals from the corrected DISPTAB (black stars) are now within ± 3 pixels ($\sim$ 7.5 km s^{-1}), while for the old DISPTAB (purple circles) they are within ± 6 pixels ($\sim$ 15 km s^{-1}).

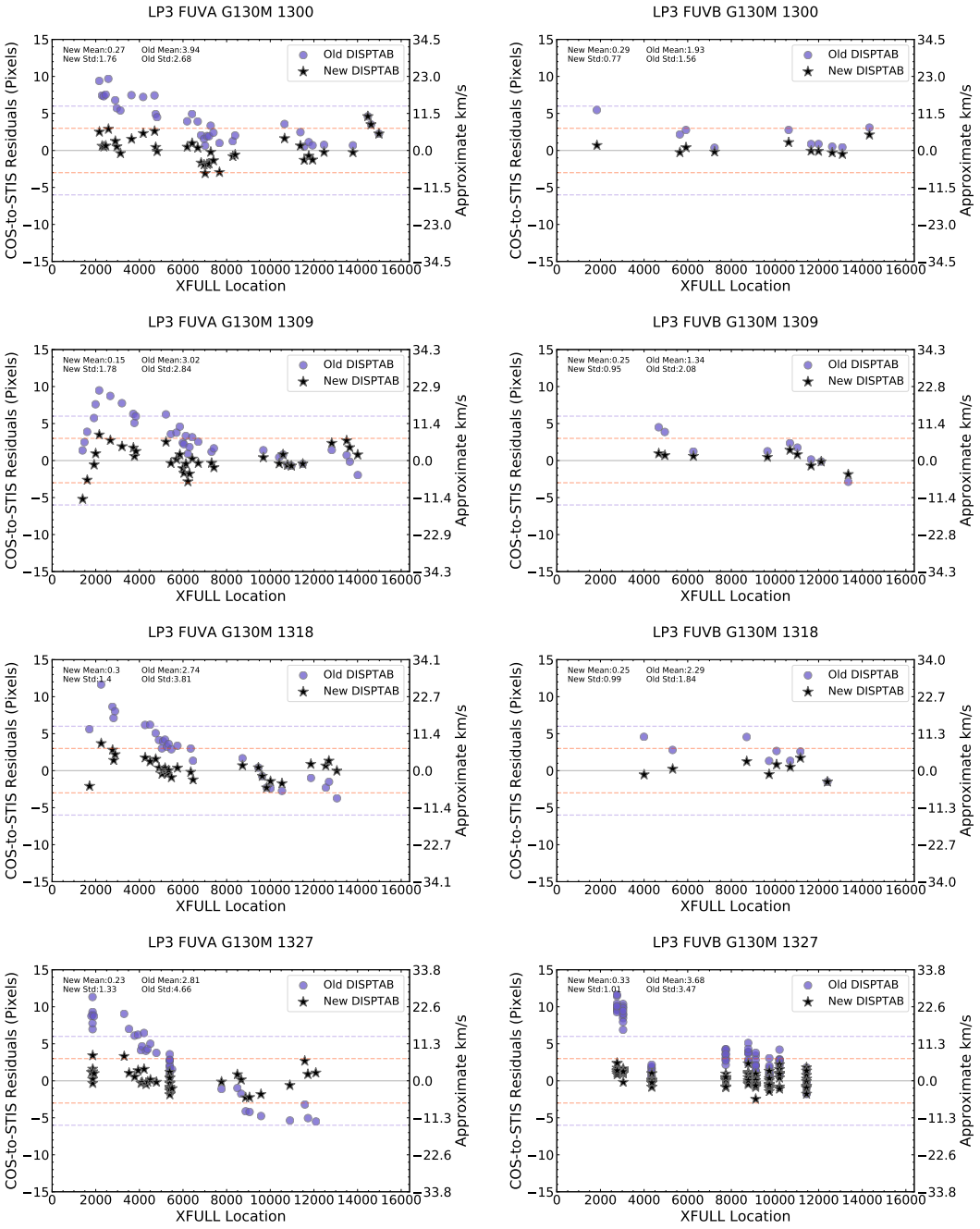

Figure 6. Continued.

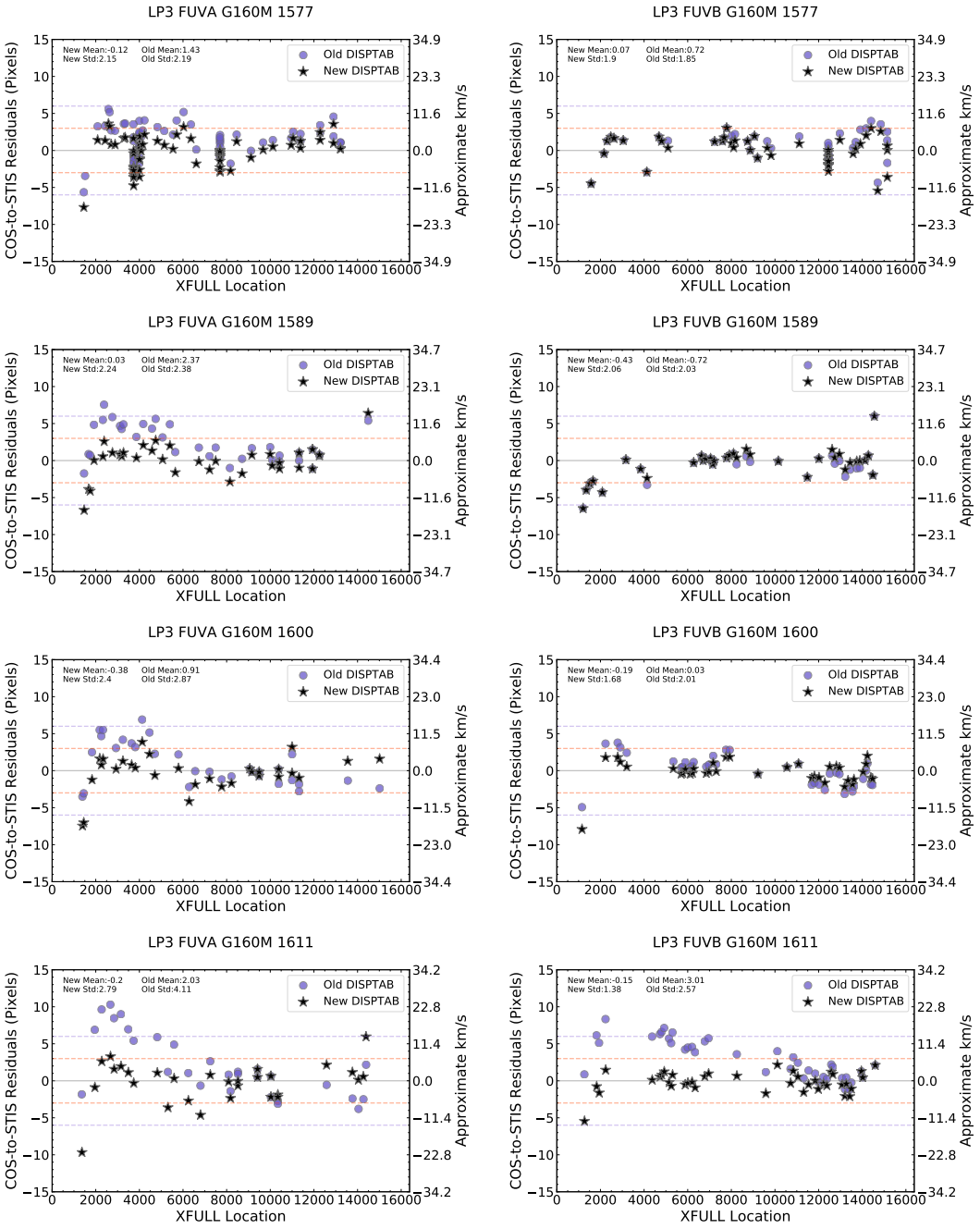

Figure 7. Same as Figure 6, but for G160M.

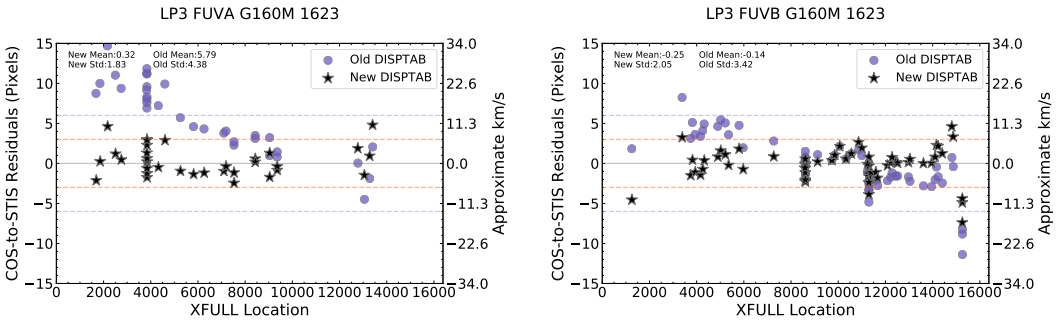

Figure 7. Continued.

4.2 COS-to-COS Comparison

Unlike for LP1 and LP2, there was not a large variety of COS data observed with different modes within a single visit with high enough signal-to-noise at LP3 to test the wavelength solutions thoroughly. Additionally, the zero points derived from the COS-to-STIS cross-correlations were believed to be already accurate enough for two reasons. First, when crafting the calibration program, the target acquisition centering errors were minimized. Second, the zero points were recomputed after the dispersion ray-trace fitting by performing the polynomial fits again but keeping the dispersion coefficients constant at the ray-trace fit values, improving the accuracy of the original derivations. Because of this, the COS-to-COS cross-correlations were performed only to check that the zero points were not significantly wrong when used on GO COS LP3 data. The cross-correlation was performed on the small subsection of LP3 data that was available, and the same techniques were used to find the zero-point offsets as in Plesha et al. (2018). The results are shown in Table 4 for G130M and Table 5 for G160M. These results indicated that the COS-to-COS distributions were already centered around zero, as expected.

Table 4. G130M Offsets from COS-to-COS Cross-Correlations

Segment	Offset (pixels)				
	1291	1300	1309	1318	1327
FUVA	0.352	0.017	0.375	−0.125	−0.099
FUVB	0.542	−0.183	0.191	0.069	−0.065

Table 5. G160M Offsets from COS-to-COS Cross-Correlations

Segment	Offset (pixels)				
	1577	1589	1600	1611	1623
FUVA	... [1]	... [1]	... [1]	−0.290	−0.996
FUVB	... [1]	... [1]	... [1]	0.311	−0.856

[1]No overlapping COS data.

4.3 Quadratic Behavior of Residuals

After applying the newly derived wavelength solutions, the residual shifts were examined in XCORR pixel space. XCORR values are the locations where photons land on the detector segment after being geometrically, thermally, and walk corrected, as opposed to XFULL values which are positions shifted to the LAMPTAB frame for wavelength assignment. Thus, residuals in XCORR space can be used to analyze artifacts related to the segment. When all of the residuals for either G130M or G160M are overlayed as in Figure 8, there is a clear quadratic trend in FUVA, along with an edge effect below XCORR $\sim$ 2000. This curvature was not seen at LP1 and LP2. Although we were meeting the half-resel ($\pm$ 3 pixel) accuracy goal with the linear fit, we also had hoped to reduce any systematic errors with the wavelength solution.

A variety of statistical tests were explored to determine the validity of this effect with observing mode, but each was inconclusive as to if the quadratic shape was significant. While these tests were ongoing, the LP4 calibration program (Plesha et al. 2019) was being planned and executed with the same target, ϵ Eri. We expected that if the same quadratic shape at LP4 was not seen (located $-5''$ from LP1 compared to LP3 located $-2.5''$ from LP1), then the quadratic shape was more likely to be caused by detector effects than by the instrument optics. For that reason, further statistical tests to define the shape of the residuals were not explored at that time. However, an investigation into the quadratic shape did ascertain that the residuals could be fit by a similar quadratic shape for both gratings, as seen in Figure 9. The similar quadratic shape for both gratings is indicative of a detector effect rather than an optical effect.

Because the LP3 wavelength calibration program (PID 14909) described in Section 2 was observed near the end of LP3 and the FUVA segment HV was not raised during that time, there was significant gain sag on the detectors when the data were taken, as seen in Figure 10. Gain sag is caused by charge depletion of the detectors with usage and leads to fewer photons converted into charge and positional errors in photon locations (Sahnow et al. 2011; Osten et al. 2013). At LP2, Ake et al. (2019) found evidence of walk at the short wavelength end of FUVA likely due to gain sag, along with uncorrected geometric distortion. Thus walk and geometric correction

errors are the prime suspects for the systematic errors for LP3. Observations at LP4, which were taken prior to the move to that lifetime position, showed no curvature in the residuals (Plesha et al. 2019), lending credence to this explanation. Since the gain varied over the period at LP3, it would be inappropriate to derive a quadratic wavelength solution from PID 14909 and apply it to earlier observations. Therefore, we decided to deliver linear LP3 wavelength solutions, just like all other lifetime positions. As shown in Figures 6 and 7, using linear wavelength solutions still meets the new accuracy goal of ± 3 pixels, even for data affected by gain sag.

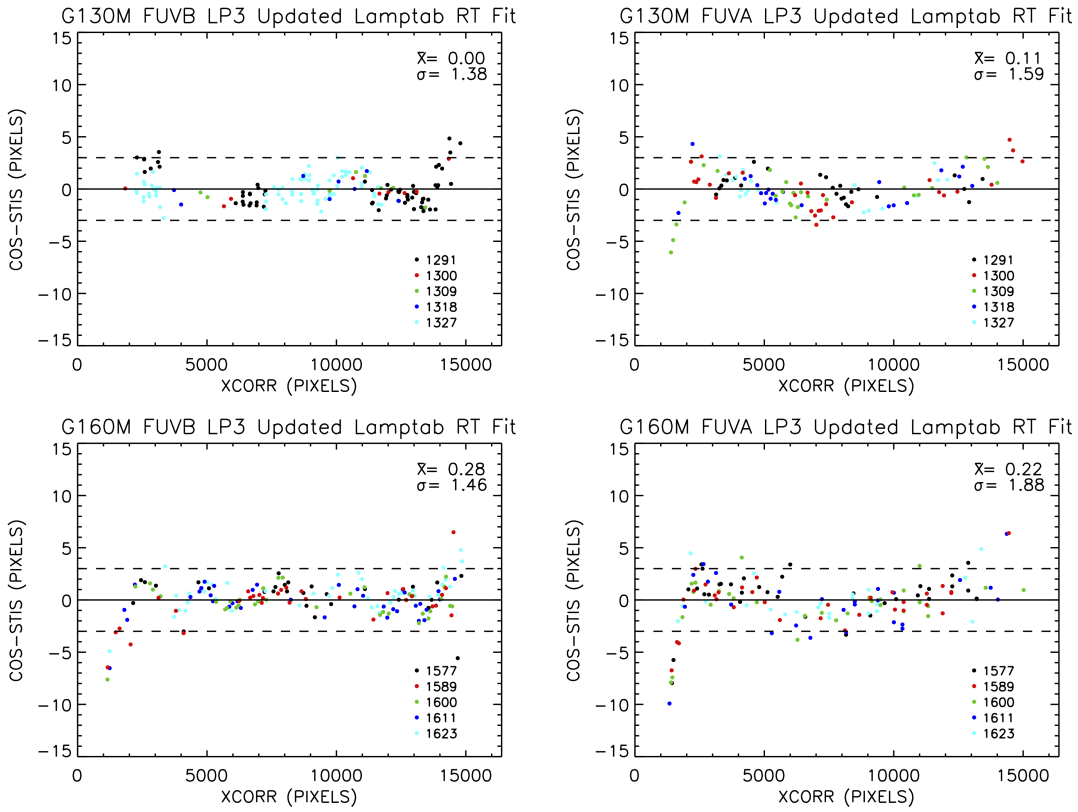

Figure 8. Residuals after applying the linear solution show a quadratic pattern for FUVA for XCORR $\gtrsim$ 2000.

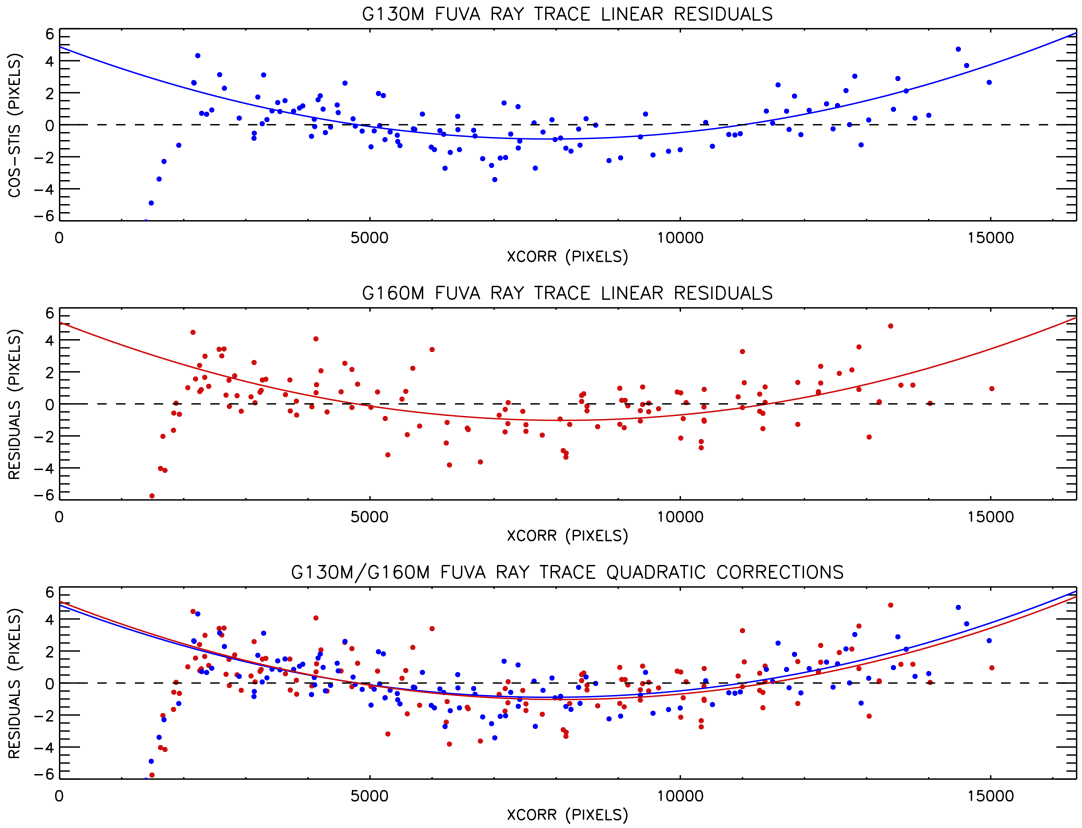

Figure 9. Quadratic fits to the G130M and G160M FUVA residuals for XCORR > 2000 (top two panels). The bottom panel shows all residuals and that the fits to the two gratings are nearly the same (blue, red curves).

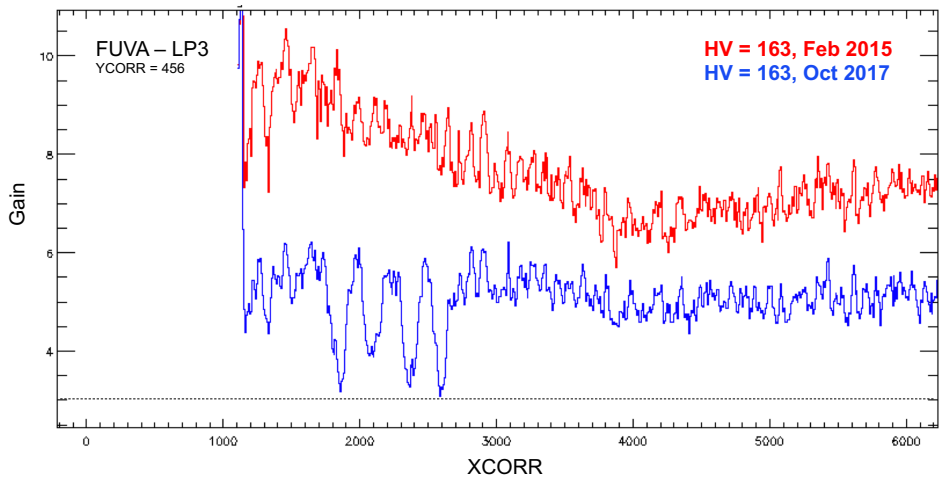

Figure 10. Modal gain versus XCORR pixel location for segment FUVA at LP3 near the beginning of the lifetime position (red) and near the end of the lifetime position (blue). The gain change at the left edge of the detector is much more significant than in the middle of the detector, supporting the claim that detector effects are causing the quadratic behavior we see in the LP3 ϵ Eri data.

5. Updates to LP3 G130M/1222

After all of the standard mode wavelength solutions for all lifetime positions were delivered, we re-evaluated some of the choices we had made. One of these choices was not updating the G130M/1222 modes except at LP4. We were aware that the original derivations of the 1222 wavelength solutions yielded a residual slope spanning a total of 6 pixels across the segments (P. Sonnentrucker, private communication). Because only $\sim 4\%$ of all LP3 datasets used the G130M/1222 setting, we could not justify at the present time to go back and obtain special data to derive 1222 solutions at LP3 as we did at LP4. However, since the G130M/1222 LP3 and LP4 focus values are within 141 steps of each other (Sonnentrucker et al. 2017), using the LP4 G130M/1222 solutions at LP3 was expected to improve the LP3 G130M/1222 wavelength solutions.

To adapt the LP4 G130M/1222 wavelength solutions for use with LP3 G130M/1222 data, we needed to take into account that the LP4 and LP3 LAMPTAB reference files were both updated using data obtained on-orbit, and therefore have unique zero-point values depending on where the Optical Selection Mechanism 1 (OSM1) stopped when rotating to the G130M/1222 position. Because the new LAMPTAB reference files were used when deriving the updated wavelength solutions, in the LP3 and LP4 DISPTAB reference files, the respective OSM1 zero points were

Table 6. G130M/1222 DISPTAB Parameters a_0, D, and a_1 for Original, Intermediate, and Updated DISPTAB Reference Files Used to Convert LP4 Wavelength Solutions into LP3 Reference Frame

Segment	Lifetime Position	File Stage	DISPTAB	a_0 (Å)	a_1 (10^{-3} Å pix^{-1})	D (pixels)
FUVA	3	Starting	xaa18189l_disp.fits	1211.28460	9.95904000	0.0
FUVA	3	Intermediate	··· [1]	1211.28460	9.95904000	−0.4188538
FUVA	4	Intermediate	··· [1]	1211.28460	9.95904000	20.2184639
FUVA	4	Final Updated	24915196l_disp.fits	1211.05934	9.96248317	0.0
FUVA	3	Final Updated	2a81746tl_disp.fits	1211.26494	9.96248317	0.0
FUVB	3	Starting	xaa18189l_disp.fits	1058.2414	9.95611060	0.0
FUVB	3	Intermediate	··· [1]	1058.2414	9.95611060	−0.03585006
FUVB	4	Intermediate	··· [1]	1058.2414	9.95611060	19.79015923
FUVB	4	Final Updated	24915196l_disp.fits	1058.0594	9.95066280	0.0
FUVB	3	Final Updated	2a81746tl_disp.fits	1058.25668	9.95066280	0.0

[1]File not delivered to CRDS.

inherently tied into the wavelength solution a_0 values. Thus we needed to find a way to separate the OSM1 zero point from the wavelength solution zero point. Fortunately, due to the way we created the new LAMPTAB reference file (E. Frazer et al. 2019, in prep.), these two zero points were already separated in an intermediate DISPTAB created in conjunction with the LAMPTAB. The OSM1 zero point was accounted for in the D value (the PSA-to-WCA offset) in the intermediate DISPTAB by subtracting the cross-correlation difference between the LP1 LAMPTAB and the new LP3 LAMPTAB from the D value in the original DISPTAB associated with the LP1 LAMPTAB. With the OSM1 zero point separated, the a_0 value was solely due to the wavelength solution zero point. The different a_0, D, and a_1 values in each of the DISPTABs used in this G130M/1222 analysis are outlined in Table 6.

Once we had all of the separated zero points, the LP4 values needed to be placed into the correct LP3 reference frame. The G130M/1222 a_1 value could be directly copied from LP4 to LP3 because the LAMPTAB only affects the zero point, not the dispersion. For the reasons discussed earlier, the a_0 value for LP4, $a_{0_{LP4}}$, needed to be converted to obtain a proper value in the correct LAMPTAB reference frame, $a_{0_{LP3\_new}}$:

$$a_{0_{LP3\_new}} = a_{0_{LP4}} - \text{ [OSM1 zero point conversion]}. \quad (3)$$

To calculate the final LP4-to-LP3 OSM1 zero-point conversion in Equation 3 (from here on, D_{LP3_new}), we needed to account for any starting offset in the D value existing in the original G130M/1222 wavelength solutions, subtract the LP4 OSM1

zero-point component, and add in the LP3 OSM1 zero-point component:

$$D_{LP3\_new} = D_{LP3\_starting} - D_{LP4\_intermediate} + D_{LP3\_intermediate}. \quad (4)$$

However, all of the values in Equation 4 in pixels, not in Angstroms. This is not an issue as long as we convert to Angstroms before applying the final transformation. To convert into Angstroms, we multiplied by the updated dispersion coefficient. Then, applying this to Equation 3:

$$a_{0_{LP3\_new}} = a_{0_{LP4}} - (D_{LP3\_new} \times a_{1_{LP4}}). \quad (5)$$

Using the values from Table 6, an example of how the calculation was done for FUVA shows that the final result is the updated a_0 value in the LP3 DISPTAB, 2a81746tl_disp.fits, which includes the updates to the 1222 wavelength solutions in addition to the other new LP3 wavelength solution updates that were delivered in the earlier LP3 file, 24914346l_disp.fits.

$$\begin{aligned} D_{LP3\_new} &= 0.0 - 20.2184639 + (-0.4188538) \\ &= -20.6373177 \\ a_{0_{LP3\_new}} &= 1211.05934 - (-20.6373177 \times 9.96248317 \times 10^{-3}) \\ &= 1211.05934 - (-0.20559893026019313) \\ &= 1211.2649 \end{aligned}$$

Testing of the updated 1222 solutions was similar to the testing of the standard modes. However, because of the limited number of observations with the G130M/1222 setting, and only the target AV 75 being observed with both COS and STIS, the testing was more restricted. We performed a cross-correlation on the LP3 COS AV 75 data to reference spectra of STIS and FUSE. Both the residuals using the original solutions derived for 1222 at LP3 and the residuals using the updated solutions derived at LP4 applied to the LP3 DISPTAB are shown in Figure 11. The residuals now no longer have a residual slope and are within the new $\pm$ 3 pixel wavelength accuracy requirement.

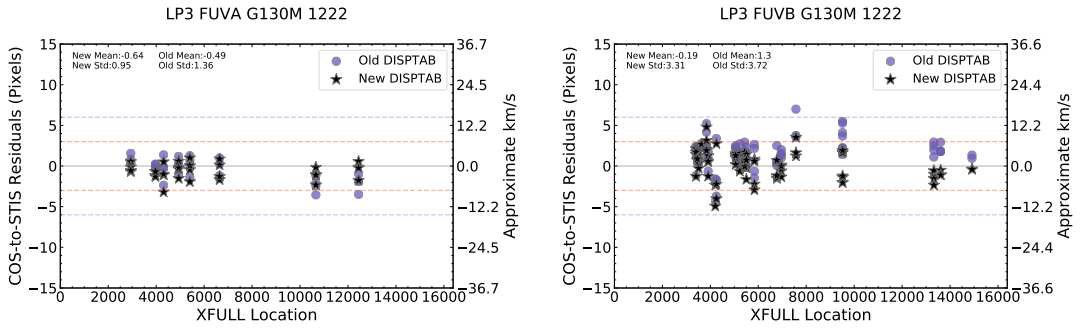

Figure 11. Same as Figure 6 for COS-to-STIS cross-correlation residuals for G130M/1222 calibrated with the LP4 solutions.

6. Reference File Details

On April 4, 2018, the dispersion relation reference file (DISPTAB) 24914346l_disp.fits was delivered in conjunction with the lamp template reference file (LAMPTAB) 24914347l_lamp.fits for use with data obtained at LP3. This DISPTAB was used from April 4, 2018 until October 8, 2018, at which point the DISPTAB containing the updates to G130M/1222, 2a81746tl_disp.fits, was delivered. File 2a81746tl_disp.fits contains the updated solutions to G130M and G160M in 24914346l_disp.fits in addition to the updated wavelength solutions for G130M/1222. Both should be used exclusively with the LAMPTAB 24914347l_lamp.fits. If these two are not used together, then there will be a zero-point offset because the DISPTAB dispersion coefficient zero point is defined in that LAMPTAB's reference frame. In the DISPTAB, the D columns and D_TV03 are set to zero for the updated modes because they were absorbed into the new zero-point coefficient. For all updated modes, the BOA values were copied from the PSA. All cenwaves are present in the new DISPTAB regardless of whether data are currently in the archive for them at LP3; G140L/1105/1280 DISPTAB coefficient values were copied from xaa18189l_disp.fits, but the D column was updated to account for the new LAMPTAB zero point from the new LP3 lamp templates created at these modes. All G130M/1055/1096 and G140L/1230 coefficient and D values were directly copied from xaa18189l_disp.fits because no DISPTAB or LAMPTAB data were obtained at these modes. A new header keyword, LIFE_ADJ, was added and set equal to 3, since this DISPTAB is only to be used at LP3.

7. Conclusions

At LP3, G130M and G160M cenwave-dependent dispersion coefficients and zero-point values have been re-derived by cross-correlating features in COS spectra to more accurate STIS data and fitting the dispersion terms to ray-trace models, as was done for the previous lifetime positions. Cenwaves G130M/1291, 1300, 1309, 1318,

1327 and G160M 1577, 1589, 1600, 1611, and 1623 were all re-derived in this way. The G130M/1222 modes were also updated with the modified LP4 wavelength solution. With these new wavelength solutions, the accuracy of the COS wavelength solution was found to be improved from $\sim$ 15 km s^{-1} (6 pixels) to $\sim$ 7.5 km s^{-1} (3 pixels). This error estimate does not include any additional errors due to target acquisition or other FUV detector effects such as walk. G140L grating wavelength solutions may need to be updated in the future, but the current wavelength accuracy of this grating (250 km s^{-1}) satisfies the scientific needs of the community, whereas the G130M and G160M gratings are more frequently used with science goals that need a more accurate wavelength scale. All archival COS LP3 data were reprocessed using the files 24914346l_disp.fits and 24914347l_lamp.fits in April 2018, and then again in October 2018 with 2a81746tl_disp.fits and 24914347l_lamp.fits. Further discussions of work on the wavelength solution improvements for other lifetime positions can be found in separate documents.

Change History for COS ISR 2018-24

Version 1: 18 March 2019 – Original Document

References

Ake, T., Plesha, R., De Rosa, G., et al. 2019, COS ISR 2018-23, "Improvements to the COS FUV G130M and G160M Wavelength Solutions at Lifetime Position 2"

Audard, M., Güdel, M., Drake, J. J., & Kashyap, V. L. 2000, ApJ, 541, 396

France, K., Loyd, R. O. P., Youngblood, A., et al. 2016, ApJ, 820, 89

Giguere, M. J., Fischer, D. A., Zhang, C. X. Y., et al. 2016, ApJ, 824, 150

Howard, A. W., & Fulton, B. J. 2016, PASP, 128, 114401

Oliveira, C., Beland, S., Keyes, C., & Niemi, S. 2010, COS ISR 2010-06, "SMOV COS FUV Wavelength Calibration"

Plesha, R., Ake, T., De Rosa, G., et al. 2018, COS ISR 2018-22, "Improvements to the COS FUV G130M and G160M Wavelength Solutions at Lifetime Position 1"

Plesha, R., Ake, T., De Rosa, G., Oliveira, C., & Penton, S. 2019, COS ISR 2018-25, "Improvements to the COS FUV G130M and G160M Wavelength Solutions at Lifetime Position 4"

Redfield, S., Linsky, J. L., Ake, T. B., et al. 2002, ApJ, 581, 626

Roman-Duval, J., Ely, J., Debes, J., et al. 2016, COS ISR 2016-01, "Optimization of Lifetime Position 3 of the COS/FUV Detector"

Sahnow, D. J., Oliveira, C., Aloisi, A., et al. 2011, Proc. SPIE, 8145, 81450Q (also COS ISR 2011-05, "Gain Sag in the FUV Detector of the Cosmic Origins Spectrograph")

Sim, S. A., & Jordan, C. 2003, MNRAS, 341, 517

Sonnentrucker, P. 2017, COS ISR 2017-07, "Cycle 23 COS FUV Internal/External

Wavelength Scale Monitor”

Sonnentrucker, P., Fox, A., Penton, S., et al. 2017, COS ISR 2017-16, “FUV Focus Sweep Exploratory Program for COS at LP4”